8. V. A. Samsonov, "Stability and bifurcation of the equilibrium of a body with a fluid," Nauchn. Tr. Inst. Mekh. Mosk. Gos. Univ., No. 16 (1971).
9. V. A. Vladimirov and V. V. Rumyantsev, "Application of Lagrange's theorem to a solid with a cavity containing a viscous fluid," Prikl. Mat. Mekh., 54, No. 2 (1990).
10. I. Gillis and B. Kaufman, "The stability of a rotating viscous jet," Q. Appl. Math., 19, No. 4 (1962).
11. R. T. Balmer and T. G. Wang, "An experimental study of internal hygrocysts," Trans. ASME, 98 (1976).

DEVELOPMENT OF SEPARATION IN THE REGION WHERE A SHOCK INTERACTS WITH A TURBULENT BOUNDARY LAYER PERTURBED BY RAREFACTION WAVES

A. A. Zheltovodov, É. Kh. Shilein, and C. C. Horstman*

UDC 532.526

The solution of many supersonic gas dynamic problems requires studying how the turbulent boundary layer interacts with various perturbations, such as shocks and expansion waves. The essential feature of such flows, compared to single interactions, is that upstream perturbations can cause downstream relaxation effects in the boundary layer. Under such conditions, relaxation properties of the flow, in particular its separation resistance, can depend on the distance from the perturbation, and also on its type and intensity.

Current research indicates that the separation properties of a turbulent boundary layer in various situations depend significantly on how well its average velocity profile is filled out. The behavior is characteristic for the development of a turbulent boundary layer on a plate [1-3]. As the Reynolds number increases to $Re_\delta \approx 10^5$, the velocity profile is observed to be less filled out and hence less able to resist separation; while the velocity profile becomes more filled out in developed flow and at higher Reynolds numbers, and hence it becomes more resistant to separation. Analogous features are noted for perturbed boundary layers in which various perturbations fill out the velocity profile. For example, theoretical analysis led to the conclusion that separation could be suppressed in accelerated flows [4]. The increase in the critical intensity of a shock in flows with boundary-layer suction and discharge has been recorded experimentally [5]. An analogous effect was observed in a turbulent boundary layer which had been perturbed by a shock [6]. According to [5], such an effect of filling out the velocity profile is explained by the total pressure growth in a characteristic wall region of the boundary layer, where its separation properties are determined. At the same time, it is obvious that in general the change in the separation properties of perturbed boundary layers can be related not only to the transformation of the average velocity profile but also to a change in the effective viscosity in the wall region. Undoubtedly the role of each of these factors should be further refined. The results of the aforementioned studies create interest in the experimental study of how a shock interacts with a turbulent boundary layer which has been perturbed by expansion waves. This situation is an extreme one for testing the use of various turbulence models in current numerical calculations.

This paper is the result of an experimental and numerical study of how a turbulent boundary layer interacts with expansion waves and a shock as it flows over wedges. The study is a combined effort of the Institute of Theoretical and Applied Mechanics, Siberian Branch, Russian Academy of Sciences (ITPM SO RAN) and NASA Ames (USA). The experiments were done at ITPM SO RAN under adiabatic surface conditions in the T-313 and T-325 hypersonic wind tunnels (cross sections of 0.6 × 0.6 m and 0.2 × 0.2 m in the working section). The models were flat wedges of fixed height h = 15 mm (for T-313) and 6 mm (for T-325) with leeward inclination angles of β = 8°, 25°, and 45°. The relatively large width of the models (b/h = 20-26.7) and the use of boundary plates eliminated three-dimensional edge effects on the flow characteristics near the plane of symmetry. Turbulent flow was developed on the horizontal surface

*NASA-Ames Research Center, Mailstop 229-1, Moffett Field, CA 94035 (415) 604-6255 Internet: horstman@whiskey.arc.nasa.gov.

Institute of Theoretical and Applied Mechanics, Siberian Branch, Russian Academy of Sciences (ITPM SO RAN), Novosibirsk. Translated from Prikladnaya Mekhanika i Tekhnicheskaya Fizika, No. 3, pp. 58-68, May-June, 1993. Original article submitted June 3, 1992.

 0021-8944/93/3403-0346$12.50

TABLE 1

M_∞	β, deg	$Re \cdot 10^{-7}$, m^{-1}	p_0, MPa	T_0, K	δ, mm	δ*, mm	δ**, mm	Wind tunnel
2,20	8—45	2,6	0,236	268±4	5,45	1,45	0,44	T-313
2,85	8	3,8	0,426	265±2	5,1	1,84	0,38	
	25	3,8	0,427	268±3	5,1	1,84	0,38	
	45	3,3	0,420	292±4	5,1	1,84	0,38	
3,80	8—45	5,8	1,068	269±2	4,9	2,04	0,29	
2,90	25	4,0	0,480	287±5	1,94	0,71	0,14	T-325

ahead of the wedge. The layer thickness δ, the extension thickness δ*, and the momentum reduction thickness δ** ahead of the depression are shown in Table 1, along with the basic flow parameters for which detailed pressure-probe measurements were made of the flows. In addition, flow patterns were recorded and surface pressures were measured over a wide range of Mach numbers ($1.9 \le M_\infty \le 3.9$) and unit Reynolds numbers ($3.5 \cdot 10^6 \le Re \le 60 \cdot 10^6$ m^{-1}) at various stagnation pressures p_0 and temperatures T_0.

The total and static pressure distributions were measured in the vertical plane of symmetry of the model by appropriate microprobes. Their orientation took into consideration the expected angles of the flow to guarantee measuring the total pressure to at least 1% and the static pressure to 5%. The pressure distribution was measured on the surface of the model along its line of symmetry with an accuracy of at least 0.5%. The generalized Crocco integral was used to calculate the velocity from measurements of the pressure field in the boundary layer. The surface friction coefficient was determined from the total velocity profiles using a method [7] based on the Ludwig–Tillman equation, which was generalized to compressible flow. The accuracy in measuring the friction coefficient was about 10%, except for regions with a high-pressure gradient where it could be as low as 15%. The flow was made visible using th Toepler method and by using an oil-black coating. The method and experimental conditions are detailed in [8].

The analytical investigations were done at NASA Ames by numerically solving the Favre-averaged transient Navier—Stokes equations for two-dimensional flow. Here an explicit-implicit finite difference method was used with a MacCormack predictor-corrector [9]. The method has second-order accuracy and satisfies the conservation laws for each computational cell. Two eddy-viscosity turbulence models were used to complete the initial equations: the Jones and Launder $k-\varepsilon$ model [10] and its modification as derived by Rodi [11].

The first model can be represented by the following basic equations:

$$\frac{D\rho k}{Dt} = \mu_t \left[S_{ij} S_{ij} - \frac{2}{3} \operatorname{div} \mathbf{u}^2 \right] - \frac{2}{3} \rho k \operatorname{div} \mathbf{u} - \rho\varepsilon + \Delta + \Lambda ,$$

$$\frac{D\rho\varepsilon}{Dt} = \frac{\varepsilon}{k} \left[C_1 \mu_t \left(S_{ij} S_{ij} - \frac{2}{3} \operatorname{div} \mathbf{u}^2 \right) - C_1 \frac{2}{3} \rho k \operatorname{div} \mathbf{u} - C_2 f_2 \rho\varepsilon \right] + \Delta + \Lambda ,$$

$$S_{ij} = \frac{\partial u_i}{\partial x_j} + \frac{\partial u_j}{\partial x_i}, \quad \mu_t = C_\mu \rho k^2 / \varepsilon .$$

Here Δ and Λ are terms that account for diffusion and for the effect of low Reynolds numbers near the wall; $C_1 = 1.44$, $C_2 = 1.96$, and $C_\mu = 0.09$ are constants [12].

The second is a two-layer model; somewhere near the wall, the differential equation for the dissipation rate ε is replaced by the algebraic equation

$$\varepsilon = \frac{k^{1,5}}{L} \left(1 + \frac{13.2}{\rho \sqrt{k}\, L/\mu} \right),$$

and the turbulent viscosity is described by the equation

$$\mu_t = f_\mu C_\mu \rho L \sqrt{k}.$$

The values of f_μ and the characteristic Reynolds number R_y are determined by the equations

$$f_\mu = 1 - \exp(-0{,}0198 R_y), \quad R_y = \rho \sqrt{k}\, y/\mu ,$$

where y is the distance along a normal from the wall.

The length scale L is described by a simple equation $L = C_r y$, where $C_r = 2.4$. This model, which can be used in the region near the wall, is joined with the first model at a distance from the wall determined by the condition $R_y = 150$ ($f_\mu = 0.95$). For $100 \leq R_y \leq 200$, changing the coordinates of the joining point changes the numerical results by 3%.

The computational grid was uniform in the longitudinal direction and, depending on the actual configuration, had from 200 to 220 cross sections, which were distributed with a spacing from 0.15 to 0.25 times the thickness of the unperturbed boundary layer. The grid was uniform along the vertical coordinate outside the flow and then became denser in a geometric progression near the wall. A total of 70-100 points was used in this direction, of which at least 30 were in the boundary layer. The minimum distance from the wall to the nearest node in each cross section was $0.05 \leq y^+ \leq 0.1$, where y^+ is a function of the wall type.

The initial conditions were determined by a uniform external flow and by the boundary layer profile in a cross section far from the interaction zone. This initial profile was obtained by calculating the flow on a plate starting from the extension thickness where the calculated variable reached the experimental value. Zero longitudinal gradients were imposed on the flow parameters at the right boundary. A no-slip condition, constant temperature, zero turbulent kinetic energy, and zero dissipation rate were imposed at the wall. A characteristic time for a calculation on a Cray YMP with one processor was about 25 min.

The basic flow development was established from detailed measurements of the pressure, velocity, and surface-shear distributions; optical visualization; and analysis of the limiting flow lines. It was shown that the basic characteristics of the flow regimes are 1) attached flow for small β's, 2) the appearance of a local separation zone in the compression corner with a free separation point at moderate β's, and 3) formation of large-scale separated flow with a fixed separation point when the β's became large enopugh – analogous to the flow around a right step. The characteristic gas dynamic curves and flow distributions on the surface for these stages are shown in Fig. 1 for $M_\infty = 2.85$.

When the slope of the leeward wedge is small (Fig. 1a, $\beta = 8°$), there are tandem attached flows, which are characteristic for isolated expansion and compression corners. The solid circles in the figure denote the outer limit of the boundary layer and correspond to a local velocity $u_\delta = 0.99u_e$ in the investigated cross sections, where u_e is the external flow velocity. Shocks and compression waves are shown by heavy and thin solid curves. The first and last characteristics of the expansion wave fan are denoted by dashed lines. The relative pressures at the surface (Fig. 1d, experimental points 1) reach the values calculated from the Prandtl–Meyer equation behind an expansion wedge and for an oblique shock wave beyond a compression corner. This correspondence occurs downstream from discontinuities in the surface by about five thicknesses of the boundary layer, which is present ahead of the discontinuities. The position of the apex of the compression corner in this and other situations is shown by arrows on the abscissa.

The local separation zone, which is characteristic for the second regime in a compression corner, is bounded by lines of divergence (separation) C and convergence (attachment) P (Fig. 1b, $\beta = 25°$). Within the thickening boundary layer, which is being compressed behind the expansion wedge, a λ-configuration of waves arises at the base of the shock. Another feature of this flow is the interaction of expansion waves with the shock inside and outside the boundary layer; as a result the shock weakens and vanishes. Moreover, the minimum relative pressure (Fig. 1d, points labeled by 2) behind the expansion corner is somewhat higher than the value calculated from Prandtl–Meyer theory ($p/p_1 = 0.101$). The error in measuring the pressure corresponds to the size of the experimental points on the figure. It is obvious that the actual pressures do not reach the calculated values behind the expansion waves primarily due to the effect of the step and the separation zone, where the increased pressure propagates somewhere over the separation point C. Increasing the Mach number or shortening the wedge strengthens this effect. A remarkable feature in the pressure distribution, which is most clearly seen at high Mach numbers (Fig. 2a, $M_\infty = 3.80$, $\beta = 25°$), is the formation of a section with a local pressure minimum at some distance from the attachment point (Fig. 2b, point 1, x = 70-75 mm). Measurements of the heat transfer rate [13] revealed a qualitatively similar variation with a similar sharp minimum behind an expansion wedge. It is obvious that this feature in the parameter distribution at the wall is caused by a centered expansion fan which starts from the triple point of the λ-configuration of shocks above the separation zone (Fig. 2a, dashed curves). The existence of such waves was confirmed by an investigation of the interference of two weak shocks of the same family [14]. The Toepler photographs of the

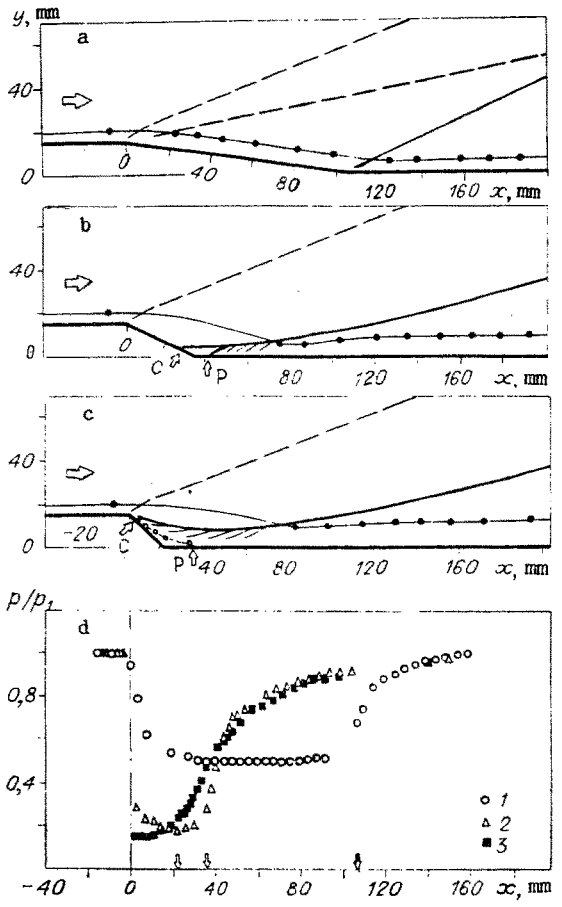

Fig. 1

flow clearly reveal that a contact discontinuity, which complements the gas dynamic flow diagram around the separation zone, propagates from the triple point (Fig. 2a, curve with dots).

As the angle is increased to 45°, the separation region increases at the compression corner, and a characteristic wave structure forms above the region (Fig. 1c). Here the separation point C tends to its limit position directly behind the apex of the expansion wedge. The distance from the apex to this point is almost independent of the Reynolds number in the range $2 \cdot 10^4 \leq Re_\delta \leq 15 \cdot 10^4$ and is roughly 1, 2, and 4 mm for $M_\infty = 2.20$, 2.85, and 3.80. The fixed position of the zero-velocity curve in the separation zone are shown by open points. This flow completely reproduces flow around a right-angle step, where the end and contact shocks combine to form an analogous wave structure at relatively high M_∞ values and moderate Re_δ values [15]. These shocks are highly distorted by their interaction among themselves and with expansion waves. The pressure distribution is qualitatively similar to flows beyond an expansion step (Fig. 1d, points 3). The relative pressure along the expansion wedge hardly changes; it corresponds quite well to that at the bottom of an expansion step, and is 0.2 for this Mach number [16].

The experimental data we obtained makes it possible to analyze how forced-flow parameters and prehistory affect the development of a separation at a compression corner, which is established in flow by perturbed expansion waves. For this purpose, Fig. 3a shows the experimental data, obtained in a flow with a free separation point behind an expansion wedge with $\beta = 25°$, on the background of correlating curve 1 for the separation length at isolated compression corners ($M_\infty = 2.20$, 2.85 and 3.80 for bands 2-4). The correlating function 1 was obtained [17] by refining earlier ones [18] and from numerous experimental data from various authors on the separation length developed in compression corners for a wide range of M_e and Re_δ. Here L_0 is the shortest distance between separation and attachment points, M_e is the Mach number in the external flow, δ is the boundary layer thickness ahead of the discontinuity, p_2 is the pressure behind the discontinuity, and p_* is the plateau pressure in the separation zone. The flow parameters ahead of the separation point were determined approximately for the interference between an expansion wave fan and a shock near the wedge. The dimensions and location of the rectangles 5 within the bands 2-4 characterize the total error in

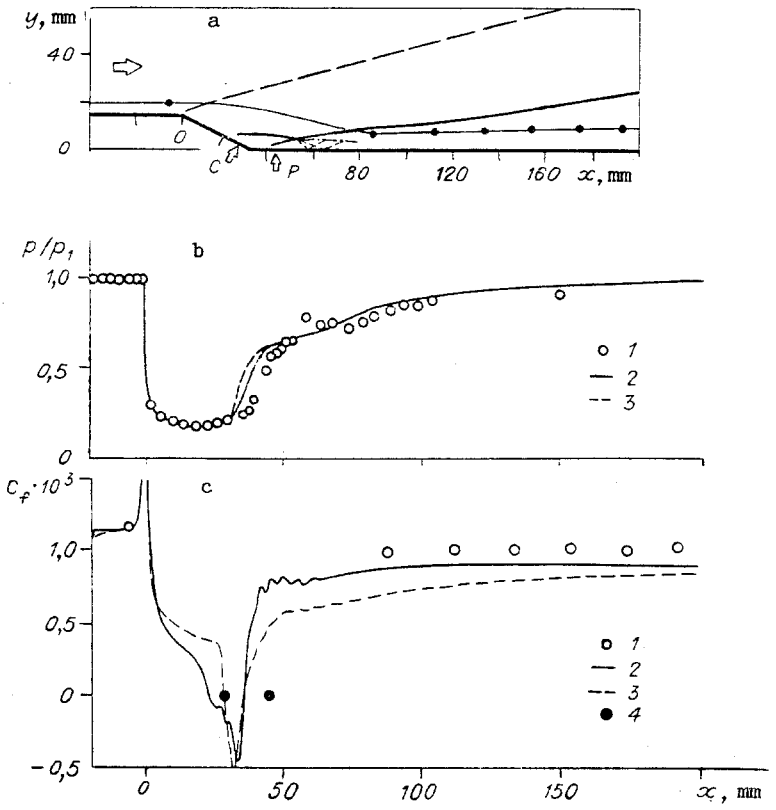

Fig. 2

determining the local values of M_e, Re_δ, and p_2/p_*. The value of δ was found from Toepler photographs of the flow, and p_* was determined from [19].

When data for a separation which has been perturbed by the boundary layer is shown in this form (Fig. 3a, bands 2-4), they are much lower than the correlation 1. This is characteristic for undeveloped separation flows, which is this case result from a significant increase in filling out the velocity profile in the preceding expansion waves. It is obvious that the separation resistance of the perturbed flow directly behind the expansion waves increases significantly and becomes similar in magnitude to the separation resistance characteristic of a flow which is relaxing a large distance behind a discontinuity [6] (Fig. 3a, points 6 and 7). The configuration examined here is a sequence of compression angles β_1 and β_2. Point 6 corresponds to $\beta_1 = 18°$, $\beta_2 = 15°$, and $M_e = 2$; point 7 corresponds to $\beta_1 = \beta_2 = 18°$ and $M_e = 2.0$ (M_e is the Mach number ahead of the second discontinuity). The data [6] for the separation length in unperturbed flow (point 8, $\beta_1 = 0$, $\beta_2 = 18°$, and $M_e = M_\infty = 2.0$) are in good agreement with the function 1. We note that in the combined flows, the increased filling out of the velocity profile results from various physical factors which occur in a relaxation flow: the acceleration of the expansion waves and the turbulence effect of the shock.

By looking only on the effects of the fullness of the velocity profile on the separation properties of the boundary layer, it is impossible to explain completely why separation develops differently in perturbed and unperturbed flows. Thus, along with the overall suppression of separation in the investigated perturbed flows, we note that the separation length increases as Re_δ decreases, as calculated from the local flow parameters behind the expansion wave fan (Fig. 3a, bands 2-4). This trend in the separation development cannot be explained by a change in filling out the velocity profile in the unperturbed flow ahead of the expansion corner, because it changes nonmonotonically for the range of Reynolds numbers in this flow ($1.5 \cdot 10^4 \leq Re_\delta \leq 25 \cdot 10^4$) and therefore has a nonmonotonic effect on the separation properties (function 1). In this regard, the observed monotonic increase in the length of the separation can evidently be explained only by a decrease in the effective viscosity in the part of the boundary layer next to the wall, due to the fact that turbulent pulsations of the expansion waves become ever more suppressed as the Reynolds number decreases. This conclusion agrees with that in [20] on how the Reynolds number affects the relaminarization of the turbulent boundary layer behind a convex corner.

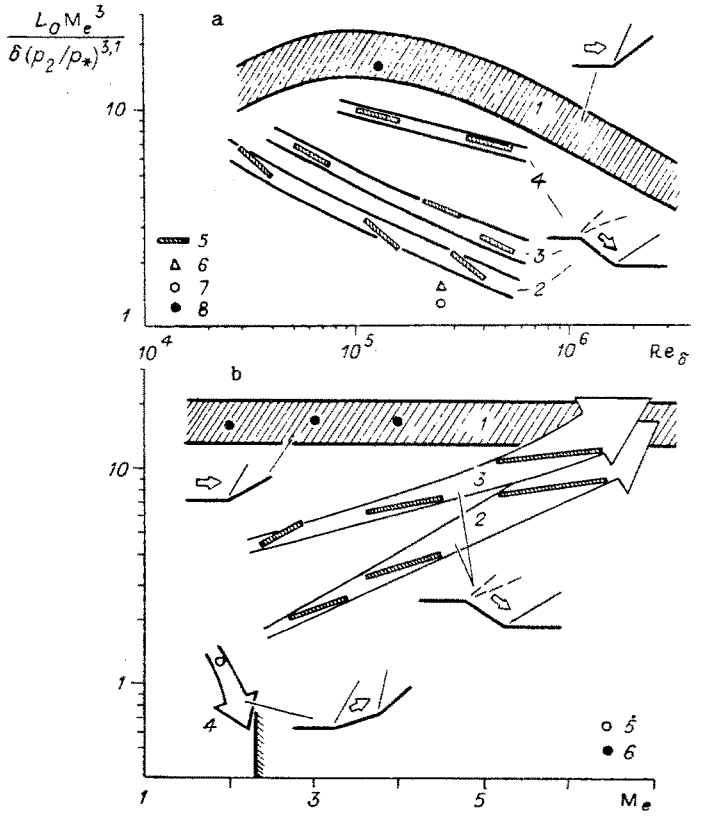

Fig. 3

Moreover, according to the data, the separation length in a compression corner behind expansion waves grows even as the characteristic Mach number increases (Fig. 3b, band 2), which is not characteristic for isolated compression corners (function 1). This behavior is unexpected, considering that the velocity profile in expansion waves [20] is filled out more (than in compression waves). Note that data (band 3) obtained on the smaller model in the T-325 wind tunnel behave in a similar fashion. Curves 1-3 are shown in Fig. 3b for a fixed $Re_\delta = 2 \cdot 10^5$.

The effect of the Mach number noted above shows up even clearer in analyzing the separation length in a dimensional form (Fig. 4). It is obvious that the behavior of L_0 behind an expansion wedge with $\beta = 25°$ and $h = 15$ mm (in Fig. 4a, the dashed band and the points 1 correspond to the M_∞ and Re_δ values shown in Table 1) contradicts the behavior characteristic for isolated compression corners (in Fig. 4b, band 1 corresponds to curve 1 in Fig. 3a, 2 is experimental data [21] and $\beta = 25°$). The observed behavior of the separation length behind the expansion wedge with a fixed angle β can be explained more effectively by the fact that the increased magnitude of the expansion wave fan suppresses the turbulence which results from increasing M_∞.

The way the separation length changes in shock-perturbed flow as M_∞ increases at a compression corner [6] (Fig. 3b, band 4) clearly contradicts the characteristic flow behind expansion waves (bands 2 and 3). The trend 4 characterizes the decrease of the separation length to zero in flow around sequential compression corners $\beta_1 = \beta_2 = 18°$ as the characteristic Mach number M_e ahead of the second step changes from 1.9 (point 5) to 2.3 (the hatched line on the axis). Flow around an analogous isolated compression corner with $\beta = 18°$ (point 6 [6]) has a developed separation all the way to $M_e = M_\infty = 4$. To all appearances, the suppression of separation beyond the step can be explained not only by the fact that the velocity profile is filled out more [6], but also by the increase in the effective viscosity due to the strengthening of the turbulent pulsations.

Thus, the investigations which were conducted indicate it is possible to suppress separation because of the greater filling out of the velocity profile in a perturbed boundary layer, both behind expansion waves and behind a shock. At the same time, one can assume that as the velocity profile is filled out due to various factors, the trend of the turbulent pulsations (down or up) can be the deciding factor in how the separated flows develop. In particular, the effect of the second mechanism (turbulence smoothing) shows up ever more clearly

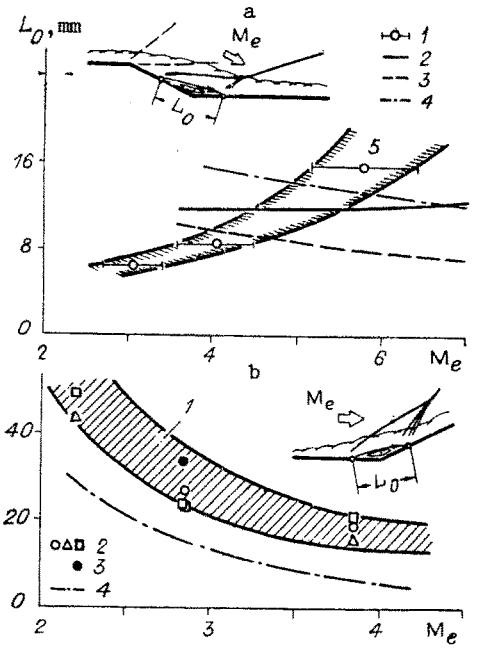

Fig. 4

with increasing Mach number on the background of the effect of the first mechanism (increased filling of the velocity profile).

There is undoubted interest in analyzing the ability of current calculational models to predict the features of separation development in perturbed turbulent flows. Numerical calculations of the Favre-averaged Navier–Stokes equations with various turbulence models have demonstrated this ability for flow around compression and expansion wedges [22]. Definite qualitative and quantitative agreement was demonstrated between experiments and calculated gas dynamic flow patterns, as well as pressure and shear distributions in the interaction zones. At the same time, additional analysis of the results shows obvious limitations of these calculations (see Fig. 4). Thus in calculations of flow over an expansion wedge (β = 25°), use of the $k-\varepsilon$ model [10] (Fig. 4a, curve 3) and the $q-\omega$ model [23] (curve 4) predict a trend of L_0 (M_e) which contradicts experiment (band 5). The calculation gives a similar trend (Fig. 4b, curve 4, $q-\omega$ model) for an isolated compression corner with β = 25°, which qualitatively agrees with the experimental correlation 1. The calculation with the $k-\varepsilon$ model (point 3), which unfortunately was done only for one Mach number, also demonstrated quantitative agreement.

It is obvious that this deficiency for an expansion wedge can be caused by various factors: peculiarities of the numerical algorithm, the degree of the grid compression, the inadequacy of the turbulence model, etc. With the goal of refining these questions, we did calculations with a very fine grid and two turbulence models. The comparison between calculation and experiment in Fig. 2b and 2c on the shear and pressure distribution at the surface for β = 25°, M_∞ = 3.8, and Re = $58 \cdot 10^6$ m^{-1} shows that the calculations done with the initial $k-\varepsilon$ model (curve 2) give better agreement with experiment than does its modification (curve 3). The main features are the better prediction of the pressure behind the expansion wave and also the notable trend to form a local minimum in the influence region of the secondary expansion waves which originate at the triple point of the λ-configuration (Fig. 2a). We also note the satisfactory agreement of the predicted friction coefficient behind the expansion wedge from the original $k-\varepsilon$ model (Fig. 2c). The calculated separation length at a compression corner, which is delimited by the separation and attachment points with $C_f = 0$, is close to that recorded by the oil-carbon black method (point 4). At the same time, the calculated position of these points is somewhat higher over the flow than in the experiment.

As can be seen from Fig. 4a (curve 2), the calculations done with the $k-\varepsilon$ model start to follow the experimentally observed trend, but do not fully agree with the experiment. However, considering the good spatial resolution of the calculational grid and also the capability of the various comparable calculational methods and models for turbulence (curves 2-4), this disagreement is associated with additional physical processes which 1) are not considered in the calculational model and 2) affected the experiment. Significant transient effects, which are characteristic of turbulent separation [24] should be considered as the

primary of such physical factors. In particular, the oil black method for visualizing the flow gives the lower bound of the location of the transient separation point. In turn, the calculational models do not consider such a complex nature of the turbulent separation directly. Predicting such fine effects requires further development of transient calculational methods based on corresponding experimental data. However, it is obvious that the stationary models investigated predict many features of the analyzed flow which are important for solving practical problems.

LITERATURE CITED

1. G. M. Elfstrom, "Turbulent hypersonic flow at a wedge compression corner," J. Fluid Mech., 53, Part 1 (1972).
2. A. B. Haines, "27th Lancaster memorial lecture, scale effect in transonic flow," Aeronaut. J., 91, No. 907 (1987).
3. L. V. Gogish and G. I. Stepanov, Separation and Cavitation Flows [in Russian], Nauka, Moscow (1990).
4. G. M. Bam-Zelikovich, "Calculating boundary layer separation," Izv. Akad. Nauk, Ser. Otd. Tekh. Nauk, No. 12 (1990).
5. D. A. Ogorodnikov, "Investigating control of the hypersonic boundary layer by suction or discharge," Technical Report 282 [in Russian], P. I. Baranov Central Scientific-Research Institute of Aircraft Engines (TsIAM) (1967).
6. M. A. Gol'dfel'd and V. V. Zatoloka, "Improving the separation properties of a turbulent boundary layer by interaction with a shock," Izv. Sib. Otd. Akad. Nauk, Ser. Tekh. Nauk, 3, No. 13 (1979).
7. M. A. Gol'dfel'd and Yu. A. Saren, "Approximate determinate of surface friction from the velocity profile of a two-dimensional compressible turbulent boundary layer," Izv. Sib. Otd. Akad. Nauk, Ser. Tekh. Nauk, 2, No. 13 (1982).
8. A. A. Zheltovodov, L. Ch.-Yu. Mekler, and É. Kh. Shilein, Features of the development of separation flow at compression wedges behind expansion waves," Preprint No. 10-87 [in Russian], Siberian Branch of the Academy of Sciences, Institute of Theoretical and Applied Mechanics, Novosibirsk (1987).
9. R. W. MacCormack, "Numerical method for solving the equations of compressible viscous flow," AIAA J., 20, No. 9 (1982).
10. W. P. Jones and B. E. Launder, "The predictions of laminarization with a two-equation model of turbulence," Int. J. Heat Mass Transfer, 15 (1972).
11. W. Rodi, "Experience with two-layer models combining the $k-\varepsilon$ model with a one-equation model near the wall," AIAA Paper N91-0216, New York (1991).
12. C. C. Horstman, "Hypersonic shock-wave turbulent boundary-layer interaction flows – experiment and computation," AIAA Paper N91-1760, New York (1991).
13. A. A. Zheltovodov, E. G. Zaulichnyi, V. M. Trofimov, et al., "Modeling heat-transfer and hypersonic turbulent separation flow processes," Modeling in Mechanics [in Russian], Vol. 3(20), No. 2, Novosibirsk (1989).
14. B. Edin, "Heat transfer on a blunt body impacted by a shock," RTK, 6, No. 1 (1968).
15. F. Khama, "Experimental investigation of a boundary shock," RTK, 6, No. 2 (1968).
16. H. H. Korst, "A theory of base pressures in transonic and supersonic flow," J. Appl. Mech., 23, No. 4 (1956).
17. A. A. Zheltovodov and É. Kh. Shilein, "Features of the development of a turbulent separation in perturbed boundary layers," Modeling in Mechanics [in Russian], Vol. 2(19), No. 1, Novosibirsk (1988).
18. D. Needham and J. Stollery, "Boundary separation in hypersonic flow," AIAA Paper N66-455, New York (1966).
19. E. E. Zukoski, "Turbulent boundary layer separation in front of a forward-facing step," AIAA J., 5, No. 10 (1967).
20. M. A. Gol'dfel'd and É. G. Tyutina, "Relaminarization of a turbulent boundary layer during rapid expansion near a corner point," Preprint No. 12-82 [in Russian], Siberian Branch of the Academy of Sciences, Institute of Theoretical and Applied Mechanics, Novosibirsk (1982).
21. A. A. Zheltovodov, É. Kh. Shilein, and V. N. Yakovlev, "Development of a turbulent boundary layer during mixed interaction with shock and expansion waves," Preprint 28-83 [in Russian], Siberian Branch of the Academy of Sciences, Institute of Theoretical and Applied Mechanics, Novosibirsk (1983).
22. A. V. Borisov and V. B. Karamyshev, "Numerical modeling of separated turbulent flows," Izv. Sib. Otd. Akad. Nauk, Ser. Tekh. Nauk, 1 (1990).

23. T. J. Coakley, "Turbulence modeling for the compressible Navier–Stokes equations," AIAA Paper N83-1693, New York (1983).
24. D. S. Dolling and C. T. Or, "Unsteadiness of the shock wave structure in attached and separated compression ramp flow fields," AIAA Paper N83-1715, New York (1983).

OPTICAL AND ACOUSTIC OBSERVATIONS OF STRATIFIED FLOW BEHIND A CYLINDER

V. E. Prokhorov, Yu. D. Chashechkin, and I. V. Voeikov

UDC 551.463.2+534.222

The shadow method, which gives highly sensitive measurements of the spatial and temporal structure of hydrophysical fields in one-component media, has been used successfully to visualize flows over experimental models. However, it is difficult to extract information on flow properties at an arbitrarily chosen point from the resultant integral picture.

The simplest method to make local measurements in a volume without perturbing it is to use remote pulsed soundings. The location and size of a specific volume can be specified by using time selection of the return signal. Ultrasonic hydrolocation (ultrasound location) is the most widely accepted pulsed sounding technique for natural causes (comparatively slow wave propagation, wavelength comparable to the inner flow scales). While it is widely used in medical diagnostics, ultrasonic location is poorly developed as an instrument for measuring the inner structure of hydrophysical fields.

The basic reason is the absence of a theoretical and empirical basis for constructing response functions which adequately describe the observed processes in terms a set of scattered acoustic signals, which in turn is explained by the transient nature of both the observed process and the scattered signals, as well as the inhomogeneity of the scatterer.

In order to establish a dependence between acoustic scattering and the flow conditions – and to identify the scatterer itself – ultrasonic soundings were made on flow behind a cylinder in water with a stratified salt concentration. The experiments were done in a tank (240 × 40 × 60 cm), which was equipped with an optical system (an IAB-458 shadow camera with a 23 cm view field), a conductometric profilometer, and a towing device for the cylinder.

The laboratory hydrolocator consisted of a receiver (a piezometric disk 2.5 cm in diameter), an output amplifier, an electronic pulse shaper, an echo signal preamplifier, a stroboscopic transformer, and a recorder. The stroboscopic transformer was required to scale the time in order to make the "fast" echo signals compatible with the inertial characteristics of the recorder. At the same time, shadow photographs were made of the flow field. The trigger signal for the camera was connected to the reference input of the recorder output.

The (salt concentration) was linearly stratified in a tank by a continuous extraction method. In these experiments, the buoyant frequency was $N = 0.6$ sec^{-1} [$N^2 = (g/\rho)d\rho/dz$, where ρ is the density, g is the acceleration due to gravity, and z is the vertical axis.] The cylinder diameter was $d = 5$ cm, the towing velocity varied from $u = 0.36$ cm/sec to 2.4 cm/sec, which corresponded to Froude numbers $Fr = u/Nd$ from 0.12 to 0.8 and Reynolds numbers $Re = ud/\nu$ from 180 to 1200 ($\nu \approx 0.01$ cm^2/sec).

Ultrasounding was done along the vertical with a repetition period of 10 msec of pulses of duration $\tau_0 = 20$ μsec and with a carrier frequency of 1 MHz (the ultrasonic wavelength was $\lambda = 0.15$ cm).

The cylinder is shown in the view field of the shadow camera in Fig. 1a (towing from left to right, $Fr = 0.67$, and $Re = 1000$). One can see the inner waves (the alternating light and dark vertical bands) ahead of the cylinder and elements of the nearby wake, including from the supporting blade, whose effects practically vanished with increasing time ($Nt > 5$).

Figure 1b illustrates the shape and location of the volume V which was irradiated with sound waves in the view field of the shadow camera. The droplet-shaped form of the volume

Moscow. Translated from Prikladnaya Mekhanika i Tekhnicheskaya Fizika, No. 3, pp. 68-74, May-June, 1993. Original article submitted April 10, 1992.

0021-8944/93/3403-0354$12.50